HIGH-PERFORMANCE COMPUTING: APPLICATIONS TO THE NUMERICAL SIMULATION OF TURBULENT FLOWS

by

Michael BREUER, Markus GLÜCK, Nikola JOVIČIĆ, and Christian BARTELS

Original scientific paper
UDC: 532.517.4:519.876.5
BIBLID: 0354–9836, *5* (2001), 1, 47–74

The present paper summarizes ongoing research and development in the field of **C***omputational* **F***luid* **D***ynamics on high-performance supercomputers at the LSTM Erlangen. Steadily increasing computer performance opens up new vistas for CFD. In the early stage, only two-dimensional predictions based on potential theory were feasible. Nowadays, solutions of the three-dimensional, time-dependent Navier-Stokes equations in complex geometries are state-of-the-art. However, still enough challenges remain for the CFD community. One of the grand challenges is the simulation of turbulent flows. Advanced techniques such as large-eddy simulation and direct numerical simulation will play a more important role in the future. Based on three different examples, the present work demonstrates, how these techniques can be applied to investigate practically relevant, turbulent flows. The examples cover a wide range of applications, namely the flow in a stirred vessel configuration, the sub- and super-critical flow past a circular cylinder, and the flow around a wing in high-lift configuration. Finally, it is exemplarily shown, how CFD can be combined with other engineering disciplines in order to solve coupled problems such as fluid-structure interaction. Based on an application related to civil engineering, the methodology and its successful application to static as well as dynamic fluid-structure interaction is demonstrated.*

INTRODUCTION

During the last decades the performance of the fastest supercomputers in the world has been increasing about one order of magnitude every five years and despite occasionally contrary prophecies this trend is still continuing (see Fig. 1). At the same time the speed of microprocessors used in PCs and workstations increases

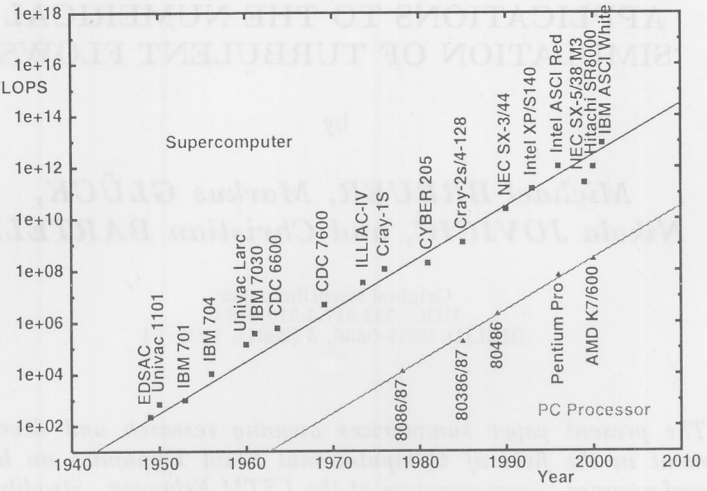

Figure 1. Development of the peak performance of supercomputers and PC processors from 1940 until today, data taken from [1–3]

roughly with the same gradient leading to the situation that CPU intensive tasks presently requiring a supercomputer can be tackled on desktop machines about 15 to 20 years later. This steadily increasing computer power and memory, augmented by concurrent progress in numerical methods, have a strong impact on the ongoing research in fluid mechanics allowing to complement and partially replace experimental investigations by numerical simulations. At first **C**omputational **F**luid **D**ynamics was critically surveyed. However, in the meantime CFD has been widely accepted as a valuable tool for performing basic research as well as for solving practically relevant flow problems.

In the beginning of the CFD era it was not possible to solve the full Navier-Stokes equations describing the conservation of mass, momentum and energy, which is a coupled system of non-linear partial differential equations (2^{nd} order in space, 1^{st} order in time). Therefore, its solutions requires high computational efforts. Neglecting all second order terms describing molecular transport processes (viscous diffusion and heat conduction) leads to the Euler equations. The solution of these still non-linear coupled system of equations is less time-consuming than the integration of the Navier-Stokes equations. For many applications, *e. g.*, in aeronautical aerodynamics such as the flow around a wing under cruise flight conditions, the solution of the Euler equations is sufficient for the determination of important quantities such as the pressure distribution. For more detailed investigations of wall-bounded flows, the Euler simulations often have been coupled with a boundary layer computation of

the near-wall flow. However, even such simulations were too costly at the beginning, demanding for further simplifications of the governing equations. Assuming an irrotational and isentropic flow, the Euler equations reduce to the potential equation which for an incompressible fluid is a single 2^{nd} order linear partial differential equation. Based on efficient and robust numerical algorithms such as the multigrid technique, the solution of the potential equation can be achieved very fast. Of course, the simplified equations can only yield reliable results as long as all simplifying assumptions are fulfilled. Because in many applications the simplification in the Euler and potential equations are not valid, a strong tendency to apply more general governing equations was observed in the following years. Nowadays, most numerical simulations in research and industry are based on the Navier-Stokes equations. Nevertheless, this does not mean that the development has come to an end. Increasing confidence in CFD leads to higher demands on this technique tending towards different goals. Some of these are:

- to increase the accuracy of the numerical solutions,
- to improve the efficiency of the numerical algorithms,
- to tackle flow problems in more complex three-dimensional geometries,
- to solve unsteady fluid flows,
- to solve coupled problems such as fluid-structure interaction or aeroacoustics,
- to include more physical and chemical phenomena such as heat and mass transfer, radiation, chemical reactions, turbulence, combustion, multi-phase flows, free-surface flows ...

The CFD group at the LSTM Erlangen has a long-lasting experience in the development of CFD codes for the solution of the Navier-Stokes equations and the application of these codes to a variety of flow problems (see, *e. g.*, [4–19]). It is involved in most of the topics mentioned above. Furthermore, the implementation of the numerical methods on high-performance supercomputers, especially parallel and vector-parallel machines, plays an important role in order to allow simulations of complex flows. Based on four different applications, the present paper summarizes ongoing research in various fields of CFD with emphasis on high-performance computing aspects, turbulence simulation based on direct numerical simulation (DNS) and large-eddy simulation (LES), and fluid-structure interaction.

The paper is organized as follows. The next section gives a brief description of the computational basics employed. The high-performance computing techniques applied are outlined in a third section. In the subsequent section, the CFD applications are described in detail and the computational results are discussed. Finally, the results are summarized and conclusions are drawn.

COMPUTATIONAL METHODOLOGY

Governing equations

A fascinating property of the Navier-Stokes equations is their capability to describe a simple laminar as well as even the most complex turbulent flow. For DNS and LES the three-dimensional and time-dependent equations have to be solved combined with appropriate boundary conditions which are defined by the flow problem of interest. If the entire spectrum of turbulent eddies is resolved by a numerical method, no turbulence model is required at all; such simulations are called DNS. On the contrary, in LES only the large energy-carrying eddies are computed directly whereas the influence of the small eddies has to be modeled by a subgrid scale model. In order to separate the large- and small-scale motions, the Navier-Stokes equations are filtered. The filtering procedure provides the governing equations for the resolvable scales of the flow field. While the continuity equation of the resolved quantities is equal to the original unfiltered one, the filtered momentum equation includes an additional term for the non-resolvable subgrid scale stresses τ_{ij} which results from filtering the non-linear convective fluxes. The tensor τ_{ij} describes the influence of the small-scale structures on the larger eddies. For incompressible flows as assumed in the present work, only this effect has to be taken into account by a subgrid scale model. Additionally, in a compressible flow, subgrid scale heat fluxes have to be considered. For DNS, the filter width tends to zero leading to vanishing subgrid scale stresses as well as heat fluxes and therefore to the unfiltered Navier-Stokes equations.

Classical turbulence modeling is generally based on the Reynolds-averaged Navier-Stokes (RANS) equations combined with statistical turbulence models. A variety of statistical turbulence models was developed to close the RANS equations on different levels of approximation. This includes simple zero-equation algebraic eddy viscosity models, most frequently used two-equation k-ε models and its numerous variants such as the k-ω- or the RNG-k-ε model, and higher-order models such as algebraic or full Reynolds stress models. As long as the flow is not too complex, these models typically provide useful results at least if the set of model parameters is adjusted properly. However, if complex flow phenomena such as separation, reattachment, transition, swirl, or streamline curvature are involved, RANS models often fail to predict the flow correctly. Nevertheless, for engineering applications, DNS and LES are often too CPU-time intensive and therefore the RANS approach has to be applied as in the case of the fluid-structure interaction problem described below and for comparison with the DNS results in the stirred vessel case.

Numerical methods

Owing to several reasons the LES and the DNS/RANS predictions were carried out based on two different computer codes which, however, have several features in common as explained below.

LES code

The LES code *LESOCC* is based on a 3-D finite-volume method for arbitrary non-orthogonal and non-staggered grids [4–9]. Block-structured grids, where the blocks may be globally unstructured but the grid in a block is locally structured, are used in the present study. The block-structured approach can be viewed as a compromise between the high geometric flexibility of fully unstructured grids and the high numerical efficiency achieved on globally structured grids. Five different options are implemented in *LESOCC* for the approximation of convective fluxes. However, based on experience in previous investigations [5,10], in most cases central differences of second-order accuracy are applied for both the convective and the viscous fluxes. In order to ensure the coupling of pressure and velocity fields on non-staggered grids, the momentum interpolation technique of Rhie and Chow [20] is applied. Time advancement is performed by a predictor-corrector scheme. A low-storage multi-stage Runge-Kutta method (three sub-steps, second-order accurate in time) is applied for integrating the momentum equations in the predictor step. Within the corrector step the Poisson equation for the pressure correction is solved implicitly by an incomplete LU decomposition method (SIP solver). Explicit time marching works well for LES with small time steps necessary to resolve turbulence motion in time. For modeling the non-resolvable subgrid scales, two different models are implemented, namely the well-known Smagorinsky model [21] with Van Driest damping near solid walls and the dynamic model originally proposed by Germano *et al.* [22] and later modified by Lilly [23]. Moreover, LES computations were performed without any subgrid scale model in order to investigate the influence of the model on the resolved scales.

DNS and RANS code

Similar to the LES code the DNS/RANS code *FASTEST* is based on a fully conservative finite-volume discretization on non-orthogonal boundary-fitted grids. Second-order discretization is used for all terms (central differences, linear interpolation) with a deferred correction approach for the convective fluxes. In contrast to the LES code, *FASTEST* applies an implicit time discretization either by a three-time-level, second-order fully implicit scheme or by a Crank-Nicolson scheme. Based on the continuity equation, a pressure-correction equation is derived according to the SIMPLE algorithm. The linearized equations for the velocity components, the pressure correction and other scalar variables are assembled and solved sequentially, where the same ILU approach as above is employed as a linear system solver. Outer iterations are performed to take into account the non-linearities, the coupling of the variables, and the effects of grid non-orthogonality, which are treated explicitly in all equations. More details on *FASTEST* are given by Durst *et al.* [11] and Durst and Schäfer [12].

One special item in connection with the stirred vessel computations should be explained here. During operation, the shape of the flow domain in a baffled stirred-

tank reactor obviously varies with time owing to the relative motion of impeller and baffles. The time-dependent solution domain inherently requires a time-dependent grid topology and solution procedure. A fully time-dependent simulation is computationally very intensive, since starting from a fluid initially at rest, up to 30 impeller revolutions have to be simulated to overcome the start-up flow patterns. An alternative approach to the fully time-dependent solution is the steady-state approach proposed by Harvey *et al.* [24] for laminar flows and extended by Wechsler *et al.* [13] to turbulent flows. As in the fully time-dependent approach, the governing equations in a domain that includes the impeller are solved in a rotating frame of reference. The governing equations in the remaining flow domain are solved in a frame of reference at rest. In contrast to the fully time-dependent approach, this is equivalent to considering only one position of the impeller relative to the baffles and corresponds to the assumption of an azimuthally constant flow field in the far-field of the impeller at some radial distance from the rotation axis of the impeller. Wechsler *et al.* [13] found encouraging agreement between steady-state and unsteady RANS computations of the turbulent flow induced by a 4/45° pitched blade impeller, whereas the steady-state computations required only a fraction of the CPU time of the fully time-dependent calculation. Hence this technique was adopted to compute the flow around a Rushton turbine by RANS and DNS.

HIGH-PERFORMANCE COMPUTING TECHNIQUES

Each year, the 500 most powerful computer systems installed worldwide are ranked by Meuer *et al.* [3] in the *TOP500 list.* The computers listed can be divided into three different categories depending on the architecture:

- **MPP Systems** = *"Massively Parallel Processing"*:
  MPP systems are built from an extremely large number $[\mathcal{O}(10^2 - 10^4)]$ of comparatively *"cheap and slow"* microprocessors (*e. g.* Pentium-Pro processor in the Intel ASCI Red MPP system).

- **PVP Systems** = *"Parallel Vector Processing"*:
  Vector-parallel processing systems such as NEC SX-4/5 or Fujitsu VPP 700/5000 are built from a moderate number $[\mathcal{O}(10^1 - 10^2)]$ of especially developed vector units applying the pipelining technique. They utilize the fastest individual processors available.

- **SMP Cluster** = *"Symmetric Multi-Processing"*:
  SMP systems are built from a cluster of symmetric (RISC based) multi-processor nodes connect via a fast network leading to a multi-level architecture. The systems consists of a moderate number of *nodes* where each node is built from

a moderate number of symmetric processors. The microprocessors belonging to one node have a shared memory. All nodes are connect by a fast network leading to fast systems. An example for such a SMP system is the German federal top-level supercomputer, Hitachi SR 8000-F1, installed at HLRB Munich [25] presently consisting of 112 nodes. Each node possesses 8 superscalar RISC processors (1.5 GFlops peak performance) having pseudo-vector properties which are achieved by extensions of the IBM POWER instruction set. These improve the memory bandwidth, alleviating the main deficit of RISC-based high-performance computing.

In the present work PVP systems and SMP clusters are prefered for the CFD simulations. Compared with MPP systems, they generally show much better performance characteristics for engineering applications.

In order to achieve high performances on vector or pseudo-vector processors, the CFD codes were adapted to these machine architectures independent of the specific vendor. According to Amdahl's law, it is extremely important to achieve a high vectorization rate. In the present CFD codes, three different types of do-loops have to be distinguished for the vectorization purpose. The first type consists of all loops which calculate the source terms and coefficients of the conservation equations for the internal flow region. Because no data dependencies exist for these kind of loops, they are easily vectorized. The vector length is determined by the number of internal control volumes (CVs) in one block which is typically larger than the optimal vector length. The second group of loops which appears in the implementation of the boundary conditions leads to much shorter vector lengths because of the restriction to 2-D surface data. Again, no recursion prevents vectorization. Larger efforts had to be made to vectorize the implicit parts of the codes, namely the SIP solver for the linear system of equations which typically consumes almost half of the computing time of the entire CFD code. Due to a recursive data structure, the SIP solver is not vectorizable in a straightforward manner. However, Leister and Perić [26] showed that vectorization can be achieved by avoiding data dependencies through indirect addressing and sweeping through the computational domain along diagonal planes, so-called hyper-planes. Thus one sweep through the entire domain consists of hyper-planes having different vector lengths. Due to this variable vector length and the indirect addressing used, the performance of the vectorized SIP solver is slightly lower than the other parts of the codes.

The parallelization strategy used in $\mathcal{LESOCC}$ and $\mathcal{FASTEST}$ for PVP systems and the node level of SMP clusters is based on domain decomposition with explicit message passing and consequently works on all kinds of machines independently of the memory architecture (distributed or shared memory). The message-passing-interface (MPI) software is used as a communication library. The domain decomposition technique is directly related to the block-structuring. The principle idea is to transform the geometric block-structure which results from the requirements to model

the geometry by some suitable mapping process to a new parallel block-structure. The resulting blocks are assigned to the available processors [11, 12]. The blocks of the parallel block-structure have to meet the most important requirement for efficient implementation on a parallel computer, namely a good load-balancing efficiency due to similar numbers of CVs on each processor. The load-balancing efficiency is defined as the ratio of the total number of CVs to the number of processors times the largest number of CVs of one processor. If the CVs are equally distributed to the processors as in the LES computations of the circular cylinder flow, the load-balancing efficiency is 100%. Typical sustained performances on four processors of a NEC SX-4 and a Fujitsu VPP 700 are about 4.0 GFlops and 3.7 GFlops, respectively. For the more complex geometry of the stirred vessel the load-balancing efficiency was about 94% in the worst case.

The SMP cluster architecture of the Hitachi SR 8000-F1 allows the use of three different levels of parallelization. The lowest level is defined by the pseudo-vector processing already mentioned above. The intermediate hierarchy level is the intra-node auto-parallelization over all processors of one SMP node supported by the compiler applying COMPAS (Co-Operative Micro Processors in single Address Space). The highest level of the parallelization hierarchy is the inter-node parallelization using several SMP nodes and a communication library for the data exchange between the nodes such as MPI in *LESOCC* and *FASTEST*. Taking all three levels into account, a total performance of about 20.8 GFlops applying 12 nodes was measured on the Hitachi SR 8000-F1 for the present computations of the airfoil flow. This is equivalent to a sustained performance of about 2.6 GFlops for each SMP node.

APPLICATIONS OF DNS AND LES

DNS of turbulent flow in a stirred vessel

Background and computational configuration

The importance of impeller stirred reactors for production processes in the chemical industry is undisputed. Operating stirred tank reactors large losses occur due to inadequate design, and further research studies are strongly recommended to increase the understanding of mixing processes in order to permit reliable process optimization. For this reason, numerous experimental investigations have been carried out. However, most of these studies are restricted to smaller scale processes, since the analysis of real full-scale equipment is often impossible. The scale-up rules which are applied to transfer the knowledge obtained on the laboratory scale are often not straightforward and uncertain leading to non-optimal design of full-scale equipment. CFD provides an advantageous and highly useful alternative for the analysis of industrial fluid flow processes.

The flow in a stirred vessel configuration often used in practice is considered in the present work. A closed, cylindrical vessel of diameter/height $T = H$ equipped with four baffles of width $b \approx T/10$ and a clearance between baffles and tank wall of $s \approx T/58$ is stirred by a Rushton turbine of the following dimensions: diameter/clearance $D = h \approx T/3$, blade width/length $w = D/5$, $W = D/4$. The geometry is similar to the configuration experimentally investigated by Schäfer *et al.* [27] except that the disc and the blades are infinitely thin. A Reynolds number of $\mathrm{Re} = \varrho N D^2/\eta = 7275$ (N = rotational speed of the stirrer) was chosen for the experiment which is accessible to DNS and RANS with standard k-ε model. Additionally, a series of lower Reynolds numbers ($0.1 \leq \mathrm{Re} \leq 4000$) was computed for the laminar and transitional mode of operation. Furthermore, RANS computations were carried out up to $\mathrm{Re} = 10^6$.

Only one half of the vessel is simulated exploiting the two-fold periodicity of the solution domain, thus significantly reducing the requirements on computational power and main memory. The underlying geometry is described by a block-structured grid with 15 blocks. The region in the vicinity of the impeller is computed in a rotating frame of reference. The grid points are clustered in this region in order to resolve the trailing vortices which emerge from the blade tips of the Rushton turbine. The total number of control volumes is about 2 million. The simulations were carried out based on $\mathcal{FASTEST}$ applying the PVP systems NEC SX-4/5 and Fujitsu VPP 700. More details on these simulations were reported by Bartels *et al.* [14,15].

Newton number predictions

The power consumption P is one of the most important parameters for the design and scale-up of stirred-tank reactors. A non-dimensional representation of P is defined by the Newton number $\mathrm{Ne} = P/(\varrho N^3 D^5)$ which for geometrically similar stirred vessels with a lid only depends on the Reynolds number Re. From experiments [28] it is known that $\mathrm{Ne} \sim \mathrm{Re}^{-1}$ for steady laminar flow ($\mathrm{Re} < 10$). For the fully turbulent regime ($\mathrm{Re} > 10,000$), the Newton number Ne remains constant and independent of Re. Between these two extremes, often close to $\mathrm{Re} = 200$, Ne exhibits a minimum.

In the following, Newton numbers calculated over a wide range of Re are compared with experimental data of Rushton *et al.* [28] and extremely careful measurements by Rutherford et al. [29] for a similar baffled stirred vessel. The geometries used in the computation and the experiments differ in one important respect. In the computation, the thickness of the blades and the disc is infinitely small, whereas in the experiments by Rutherford *et al.* [29] Ne was measured for different but finite blade thicknesses. In the experiments by Rushton *et al.* [28], the thickness is unknown, but photographs [28] suggest relatively thick blades. The results of Rutherford *et al.* [29], which show that Ne increases with decreasing blade thickness, allow the conclusion that the Newton numbers reported by Rushton *et al.* [28] for the Rushton turbine

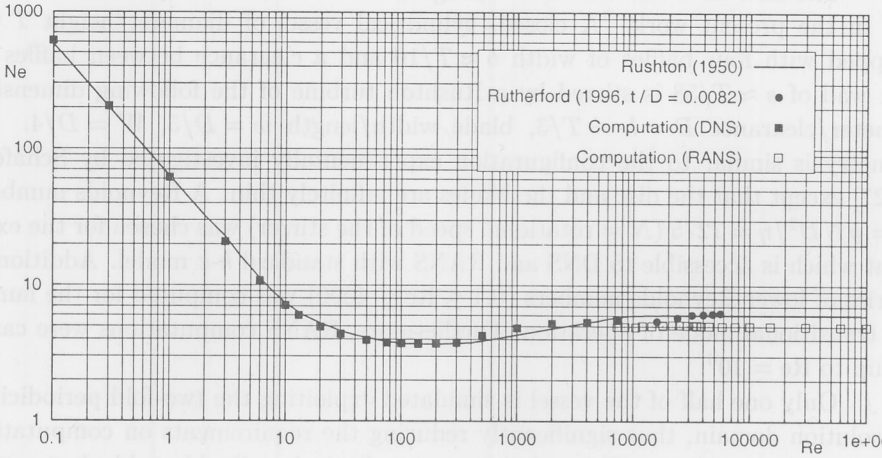

Figure 2. Computed Newton number Ne vs. Reynolds number Re for the vessel stirred by a Rushton turbine and comparison with experimental data by Rushton *et al.* [28] and Rutherford *et al.* [29]

may be too high, since even for the blades with the smallest thickness considered in Rutherford *et al.* [29] ($t/D = 0.0082$) the Newton number in the plateau region hardly exceeds the level of Rushton's results of Ne = 6. For thicker blades a Newton number around or below Ne = 5 is found.

The comparison of computed and measured Newton numbers is shown in Fig. 2 as a log-log plot. For the DNS, the overall agreement with the measurements is good except for a minimal underprediction of Ne for $10 < \mathrm{Re} < 100$ and a premature increase in Ne in the calculation from the minimum around Re = 200 towards a constant value in the fully turbulent regime. Moreover, the Newton number seems to level off at a slightly lower value (about 7%) than indicated by experiments of Rushton *et al.* but is still above the results of Rutherford *et al.* Additional RANS calculations based on the standard k-ε model capture an almost constant value of Ne in the range $12,000 < \mathrm{Re} < 10^6$. Nevertheless, the error of the predicted Newton numbers is higher (about 17% compared with the experiments of Rushton *et al.* [28]) than in the DNS. This additional error is probably due to deficiencies of the k-ε model used.

Flow field predictions

At Re = 7275 the flow in the vessel is in the turbulent regime. For this case a DNS was carried out. For comparison the flow was also predicted based on a RANS simulation with the standard k-ε model. The instantaneous as well as the

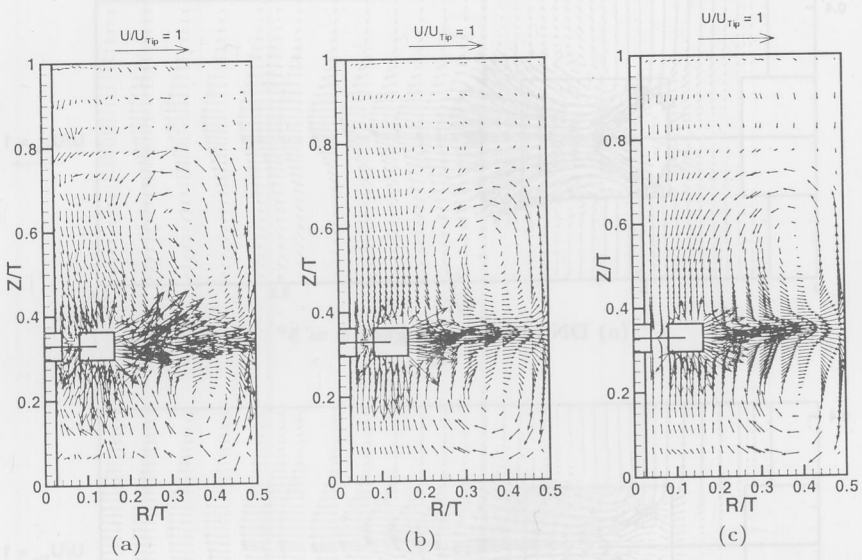

Figure 3. Computed velocity vectors in the mid-baffle plane, Re = 7275; (a) DNS: instantaneous, (b) DNS: time-averaged, (c) RANS with k-ε model

time-averaged flow patterns in the mid-baffle plane for the DNS (averaged over 8.24 revolutions) and the k-ε prediction are depicted in Fig. 3 (a)–(c). In all three subfigures, the two ring vortices driven by the radially propelled fluid are visible. It is also obvious that the lower vortex reaches the bottom of the vessel in all cases whereas the upper ring vortex does not extend up to the lid of the vessel. A closer comparison of the time-averaged DNS and the k-ε model results reveals slight differences: The position of the two ring vortices is shifted in outward direction for the simulation with k-ε model. Whereas the centers for the DNS are at $R/T = 0.355/0.37$ for the upper/lower vortex, respectively, the centers are at 0.38 and 0.395 for the k-ε result. In the DNS, the upper ring vortex does not extend up to the same height as in the RANS calculation. In the DNS, the upper limit of the vortex is 0.71 and in the RANS calculation it is about 0.75.

The flow field in the vicinity of the agitator blades is depicted in Fig. 4. The flow pattern in the plane of the blades itself does not exhibit any significant difference of the two approaches. A comparison of the RANS and the DNS results in a plane at an angle of $\phi = 5°$ behind the blades (Fig. 4) reveals two important differences: The vortex roll-up behind the inner part of the blades, forming some kind of recirculation zone, has a much larger extent in the DNS results compared to the RANS results. The location of the two *"tip"* vortices that form at about 5° behind the blades, is also

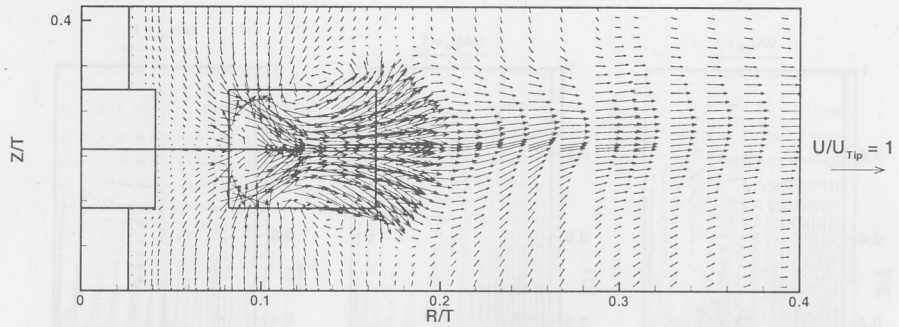

(a) DNS time-averaged: $\phi = 5°$

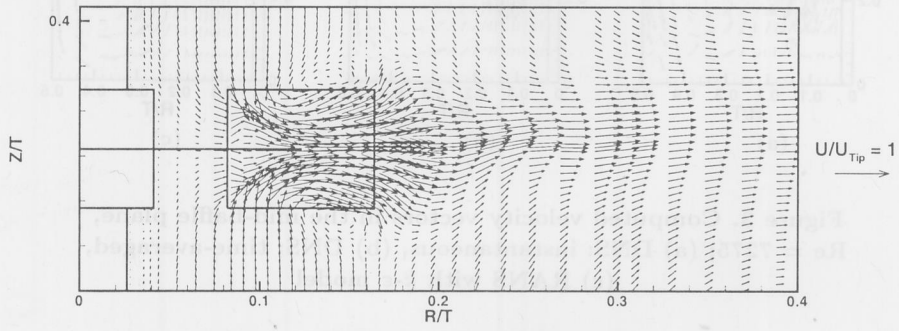

(b) RANS with k-ε model: $\phi = 5°$

Figure 4. Impeller flow field at $\phi = 5°$ behind the blade, direction and magnitude of the velocity vectors at Re = 7275; (a) DNS time-averaged, (b) RANS k-ε prediction

closer to the axis in the DNS. Both simulations show the distinct upward inclination of the flow field discharged from the impeller. The instantaneous DNS flow field (not shown here) depicts a very interesting, wavy flow structure of the radial impeller flow, indicating a Kelvin-Helmholtz instability. A close comparison of the time-averaged DNS and RANS results of the discharge flow field shows that the flow pattern of the RANS simulation is a little more wavy than that of the DNS results. The flow structure predicted by DNS receives strong support by experimental findings [30].

The flow field in a plane at an angle of $\phi = 15°$ behind the blades (not shown here) is characterized by the two tip vortices that were already present in the plane $\phi = 5°$ behind the blades but meanwhile have been transported in radial direction by the large-scale flow field. It is interesting that the location of the vortices in the DNS results is now farther away from the axis compared with the RANS results

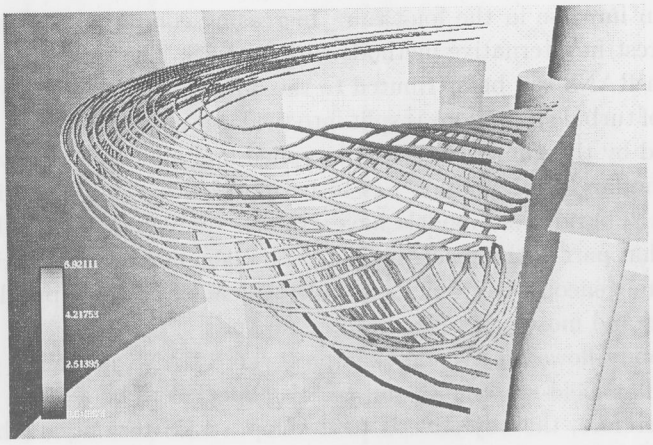

Figure 5. Streaklines starting behind a blade of the Rushton turbine and distribution of the turbulent kinetic energy, RANS computation

(especially for the lower vortex) indicating that the speed at which the vortices have been convected outwards is much higher for the DNS. A second interesting difference is that the vortices in the DNS are much closer to the plane of the disc (despite the same initial distance in the 5° plane). The radial offset of the two vortices in the DNS and the smaller distance of the vortices to the plane of the disc is in agreement with experimental findings. The two tip vortices are dying out at an angle of about $\phi = 35°$ behind the blade. This result is almost identically produced by the DNS and the RANS simulation.

The vortical structure behind the impeller blades is more clearly visible in a 3-D visualization shown in Fig. 5 for the RANS computation depicting streaklines with seed positions directly located behind a blade and rotating with the same angular velocity as the impeller. They reveal the formation of the two trailing vortices behind the blade, one above and one below the impeller plane. The vortical region is restricted to a relatively small distance behind the blade. More details of these investigations and a comparison of the distribution of the turbulent kinetic energy can be found in Bartels *et al.* [14,15].

LES of circular cylinder flow

Background and computational configuration

As described above, statistical turbulence models often fail to predict reasonable results if complex flow phenomena are involved. Therefore, the RANS approach

seems to be an impasse in the long run. Increasing computer performances led to increased interest in alternative methods such as LES. The main advantage of LES compared with RANS can be attributed to the different underlying concept. In LES the spectrum of turbulent motions is split into the large energy-carrying vortices which can be resolved by the numerical method applied and all small scale vortices. Their influence on the large scale motion has to be modeled by an appropriate approach. However, such subgrid scale models have a much simpler task than RANS models because only that part of the spectrum has to be taken into account which is assumed to be more homogeneous, isotropic, and independent of the flow problem leading to straightforward and more generally accepted models.

Bluff body flows are typical examples where RANS modeling generally fails to predict the flow field reasonably and LES is expected to be a much more suitable approach. Therefore, the objective is to develop a LES technique which is able to simulate such flows especially at high Reynolds numbers [4–7, 9]. In order to reach this goal, it is necessary to validate the physical models and the numerical methods applied by detailed investigations based on well-documented test cases such as the flow past a circular cylinder. Especially at high Reynolds numbers, the cylinder flow can be considered as the paradigm of complex flows, because it involves remarkably complex flow features such as thin separating shear layers, transition and large-scale vortex motion in the wake. Therefore, successful applications for this test case can be considered as the *admission to real world applications* of LES.

First, a low sub-critical Reynolds number of Re = 3900 was chosen. It is known from experiments that for this Reynolds number, transition takes place in the free shear layers. Much more challenging is the high-Re case of Re = 140,000 investigated afterwards. At this Reynolds number the flow is again sub-critical, *i. e.* the flow in the boundary layers is still laminar at the separation point and transition takes place in the free shear layers. In the wake vortex shedding is observed. Compared with the low-Re case the boundary layer is about six times thinner ($\delta \sim 1/\sqrt{\mathrm{Re}}$). Nevertheless, to avoid any kind of wall functions, the boundary layer is resolved by extremely fine grids in the near-wall region and no-slip boundary conditions are applied. In the spanwise direction of the cylinder, periodicity of the flow is assumed. At the inflow plane, constant velocity is imposed [5–7]. A convective boundary condition is used at the outflow boundary. Various curvilinear, O-type grids are generated for this investigation with up to 6.76 million control volumes. In all cases the grid points are clustered in the vicinity of the cylinder wall and in the wake region. More details of the grids were given by Breuer [5–7, 9]. The computations were carried out using two different PVP systems (NEC SX-4 and Fujitsu VPP 700) and one SMP system (Hitachi SR 8000-F1).

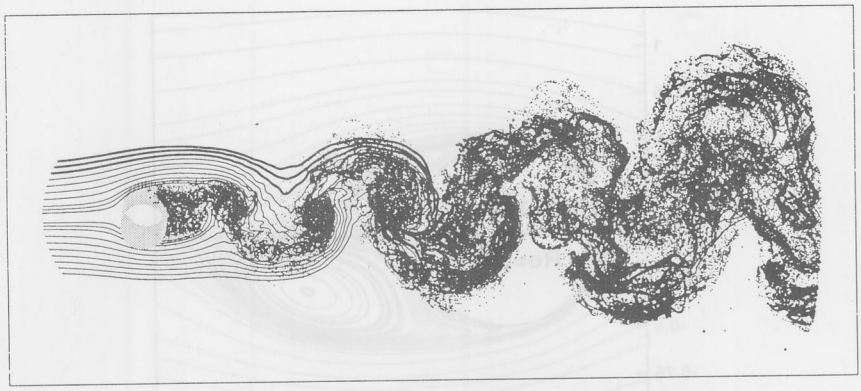

Figure 6. Von Kármán vortex street past a circular cylinder visualized by streaklines for Re = 3900, flow computed by LES

Unsteady and time-averaged flow field

Figure 6 shows a snapshot of the turbulent von Kármán vortex street past the cylinder at Re = 3900 visualized by streaklines. Weightless particles released at 20 different positions on a vertical line in front of the cylinder were integrated during the flow computation. Of course, the particles do not remain in the one plane. After transition has taken place in the free shear layers of the cylinder, they are spread out in the entire integration domain forming a complex three-dimensional flow structure in the wake. At Re = 3900 the Strouhal number of the vortex shedding frequency was found to be within the experimental range of St = 0.215 ± 0.005 determined by Cardell [31]. For the high-Re case, St varies around 0.2 for most of the computations based on different grids and different SGS models applied. This agrees fairly well with experimentally determined St values in the literature.

In accordance with experimental measurements, the time-averaged flow field for Re = 3900 consists of a large recirculation region behind the cylinder and two additional, small separation bubbles attached to the downstream face of the cylinder. Figure 7 reveals a direct comparison of the streamlines for both sub-critical Reynolds numbers. In contrast to the low-Re case, no small counter-rotating vortices attached to the backward side of the cylinder can be observed at high Re. Furthermore, the recirculation region behind the cylinder is much shorter for Re = 140,000.

Figure 8 shows a zoom of the time-averaged velocity field in the vicinity of the apex of the cylinder at Re = 140,000. The thin boundary layer is resolved in this region by about $25 - 30$ grid points on the finest grid used. In order to prove that the boundary layer separates in the laminar mode, one possibility is to consider the predicted distribution of the turbulent kinetic energy k (Fig. 8), which clearly demonstrates that k is zero up to the apex of the cylinder. Hence, separation takes

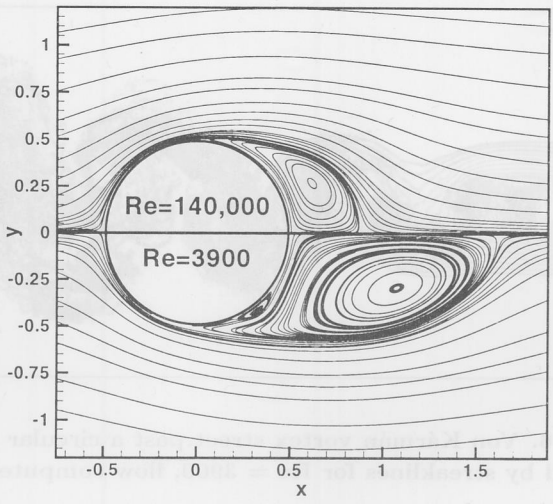

Figure 7. Comparison of the time-averaged streamlines for the sub-critical flow past a circular cylinder at two different Reynolds numbers; upper part: Re = 140,000, lower part: Re = 3900

place in the laminar mode as experimentally expected for a sub-critical Re forming free shear layers. An immediate transition to turbulence close to the cylinder is observed accompanied by a very short recirculation region. Compared with the low-Re case, transition to turbulence moves farther upstream.

In experimental investigations Cantwell and Coles [32] determined a drag coefficient of $C_d = 1.237$ at Re = 140,000. However, it is well known that C_d depends not only on the Reynolds number but on a variety of influencing factors such as the aspect ratio of the cylinder, the blockage ratio of the cylinder in the wind or water tunnel, or the end conditions. This typically leads to highly scattered experimental data such as the data collection of Cantwell and Coles [32] clearly demonstrates. For LES on a coarse grid, the predicted time-averaged drag coefficients were found to be $C_d = 1.218$ and 1.239 for the Smagorinsky and the dynamic model, respectively. Grid refinement leads to a slightly increased value for the Smagorinsky model ($C_d = 1.286$), whereas the drag coefficient for the dynamic model increased to $C_d = 1.454$. For a more detailed comparison with measurements including profiles of velocity components and higher-order turbulence statistics, we refer to the thorough studies on numerical and modeling aspects for the low-Re case [5,9] and the high-Re sub-critical case [6,7,9].

Finally, it is demonstrated that the present methodology also allows to compute the super-critical cylinder flow. For this purpose, Fig. 9 shows the turbulent flow

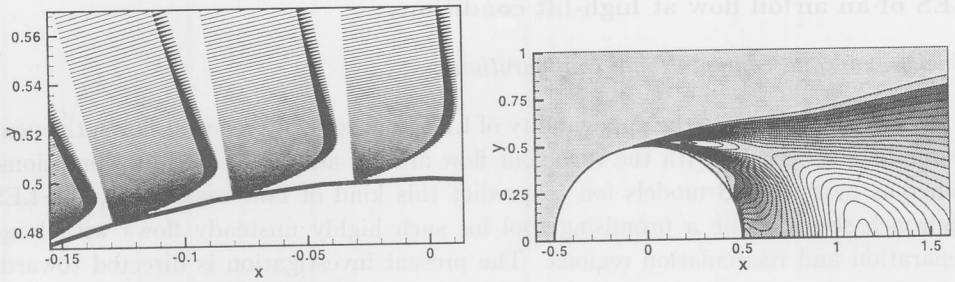

Figure 8. Time-averaged flow field past a cylinder at Re = 140,000: zoom of the boundary layer near apex of the cylinder (left) and contours of turbulent kinetic energy k (right)

past the cylinder at Re = 10^6 computed by LES. In contrast to the previous cases transition now takes place within the attached boundary layer at the cylinder. This leads to a strongly reduced drag coefficient C_d (factor of about 3) and much smaller amplitudes of the C_d and C_l oscillations. This is visible in the visualization of the flow field shown in Fig. 9, where the vortex shedding phenomenon completely disappears in the vicinity of the cylinder. Farther downstream quasi-periodic structures can still be observed in the far wake. The time-averaged flow field (not shown here) shows that the separation point is now at $\Theta_{Sep} = 131° - 137°$ which is about 40° postponed compared with the sub-critical case and explains the reduced drag coefficient. In general, all described features are in close agreement with experimental observations. The simulations have shown that the LES technique is a powerful tool especially for complex, statistically unsteady flows and will partially replace RANS predictions in the future.

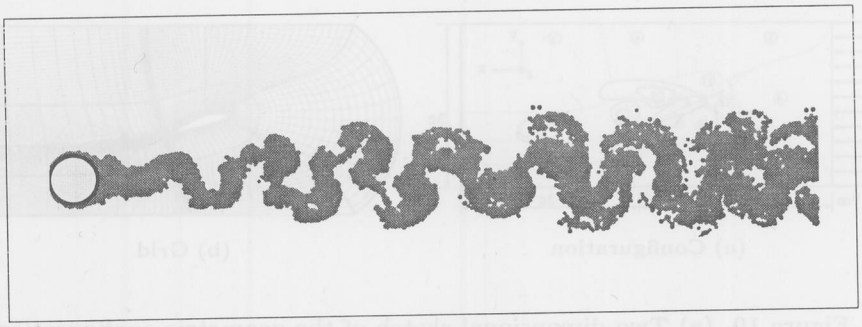

Figure 9. Super-critical flow past a circular cylinder visualized by streaklines for Re = 10^6, flow computed by LES

LES of an airfoil flow at high-lift conditions

Background and computational configuration

To demonstrate the applicability of LES to practically relevant flows, the next example is concerned with the turbulent flow around airfoils at high-lift conditions. Whereas most RANS models fail to predict this kind of flow reasonable, the LES approach seems to be a promising tool for such highly unsteady flows with large separation and recirculation regions. The present investigation is directed towards a configuration experimentally investigated within the COSTWING experiment by Lerche and Dallmann [33]. An unswept airfoil based on a NACA-4415 profile is mounted inside a channel (see Fig. 10a). The Reynolds number in the experiment ranges from $\mathrm{Re}_c = 8 \cdot 10^4 - 8 \cdot 10^5$ with $0° \leq \alpha \leq 22.5°$. A primary objective of the COSTWING experiment is to serve as a database for the validation of numerical simulation techniques. In this sense it is used for the present numerical investigation where the main goals are to study the physics of stalled airfoil flows in detail. Because experimental measurements are not yet available, this study first concentrates on a lower Reynolds number ($\mathrm{Re}_c = 20,000$) which will be increased systematically in the ongoing project. The angle of attack is currently fixed to $\alpha = 18°$ where leading-edge separation takes place at the airfoil.

The NACA-4415 profile is mounted inside a plane channel of height $3\,c$, where c describes the chord length of the profile. Upstream of the profile the channel has a length of $2\,c$, whereas downstream a length of $3\,c$ is assumed (see Fig. 10a). At the Re_c chosen, no-slip boundary conditions can be applied at the surface of the profile. In order to save grid points the boundary layers of the channel walls are not resolved and approximated by slip-conditions ($\partial u/\partial y = v = \partial w/\partial y = 0$). Owing to this channel configuration a lot of grid points can be saved because the far-field

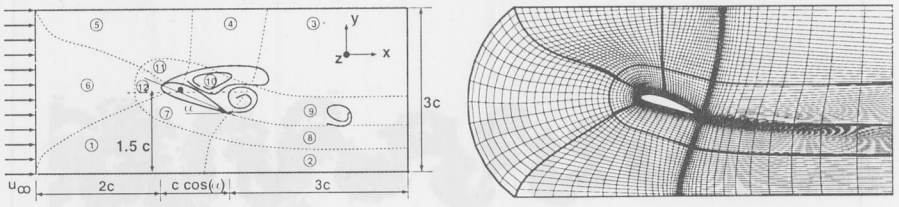

(a) Configuration (b) Grid

Figure 10. (a) Two-dimensional sketch of the geometric configuration including block boundaries; (b) x-y-plane of the grid (only every fifth grid line is shown)

does not have to be resolved. The experiment was especially designed in such a way that either statistically two-dimensional or spanwise periodical flow structures can be expected. Therefore, periodicity in the spanwise direction is assumed and a spanwise computational domain of depth $z_{max} = 1.0 \cdot c$ is chosen. This choice is based on a detailed investigation for the flow around an inclined flat plate at the same flow conditions (Breuer & Jovičić [18]) demonstrating that this spanwise extension is on the one hand necessary to assure reliable results and on the other hand represents a well-balanced compromise between spanwise extension and spanwise resolution. At the curved inlet section a constant velocity u_∞ is prescribed, whereas at the outlet a convective boundary condition assures that vortices can pass through the outflow boundary [5].

A curvilinear block-structured grid consisting of 12 blocks with a total of $\approx$8.34 million control volumes (76 CVs in spanwise direction) is applied (see Fig. 10b). The grid points are clustered in the vicinity of the airfoil and at the trailing edge. The smallest control volume has an extension of $0.001\,c$ in wall normal and mean flow direction. Along the lower surface of the profile and the nose region 100 and 60 grid points are used, respectively. The leeward side, which is the region of main interest for the present study, is resolved by 200 grid points along the surface. The simulations were carried out on the SMP system Hitachi SR 8000-F1, applying 12 nodes (= 96 processors).

Unsteady and time-averaged flow field

Figure 11 depicts the dynamics of the flow past the airfoil by contours of the vorticity component ω_z. Quasi-periodic vortex shedding can be observed from the trailing edge of the profile. The LES results show that the entire flow field is strongly dominated by the development and shedding behavior of these trailing-edge vortices. The Strouhal number of the shedding cycle is $\mathrm{St} = fc/u_\infty = 0.636$ or $\mathrm{St}' = fc \cdot \sin\alpha/u_\infty = 0.197$, when scaled with the windward width. Four different phases (a–d) with a time increment of about 0.56 dimensionless time units are shown in Fig. 11 representing slightly more than one typical vortex shedding cycle ($\Delta T_{cycle} \approx 1.57$). During its initial phase (a) this vortex is attached to the trailing edge of the airfoil while vorticity is accumulated in it being fed by the corresponding shear layer. The vortex size is continuously increasing (b). After it has reached a certain diameter (b–c), the vortex is shed and convected downstream, while diffusion of vorticity takes place (c–d). Then a new shedding cycle begins.

The typical flow structure is also visible in the spanwise and time-averaged flow field ($\Delta T_{avg} = 80.$) shown in Fig. 12. As expected, the flow separates shortly after the leading edge induced by a strong positive pressure gradient in this region. It forms a large clockwise rotating recirculation region on the leeward side of the airfoil. Behind the trailing edge the strong counterclockwise rotating vortex structure is clearly visible which plays an important role for the dynamics of the entire flow field.

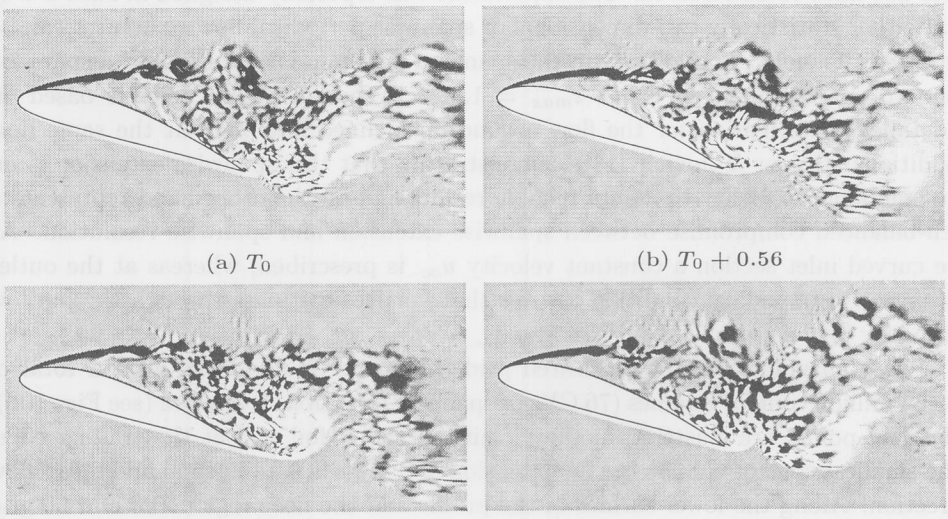

(a) T_0 (b) $T_0 + 0.56$

(c) $T_0 + 1.12$ (d) $T_0 + 1.7$

Figure 11. Vortex shedding cycle past the inclined airfoil at $\alpha = 18°$ and $Re_c = 20{,}000$, contours of vorticity ω_z at four different phases, $\Delta T_{cycle} \approx 1.57$

In a previous study for an inclined plate (Breuer & Jovičić [18]), it was shown that a sufficiently large spanwise extension of the domain is required to guarantee a reliable simulation. Provided that this condition is fulfilled, the trailing-edge vortex in the time-averaged flow is located behind the profile (Fig. 12a) or the plate, respectively. However, if the spanwise extension is too small in the LES calculation or in the extreme case a two-dimensional configuration is considered, the trailing-edge vortex resides upon the end of the profile (not shown here). Hence for both configurations the same behavior is found.

In addition to the strong shear layer developing at the trailing edge, a second one of weaker strength is generated near the leading edge. The flow separates from the curved profile forming a free shear layer in which a Kelvin-Helmholtz instability and transition are detected in the instantaneous flow field. Furthermore, fluid circulation in clockwise direction is observed leading to the large recirculation region on the leeward side of the airfoil (see Figs. 11 & 12). A nearly constant pressure distribution is found in the separation region on the leeward side. However, no regular shedding motion of vortices generated at the leading edge is visible. The size of the attached clockwise rotating recirculation region is depending on the presence, the size and the strength of the counterclockwise vortex structure arising at the trailing edge.

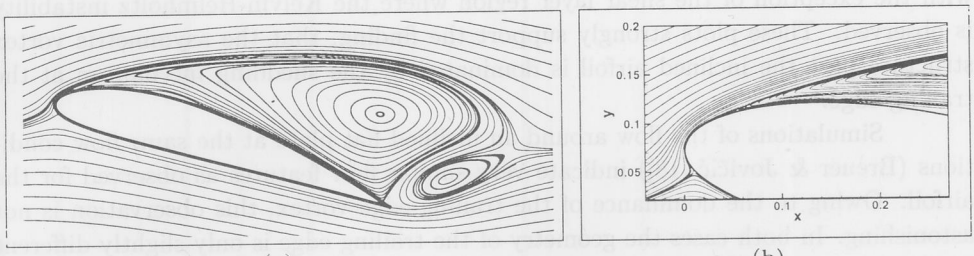

(a) (b)

Figure 12. Streamlines of the time-averaged flow, $Re_c = 20{,}000$, $\alpha = 18^\circ$, $z_{max} = 1.0 \cdot c$; (a) flow past the NACA-4415 profile, (b) zoom of the nose region

While the counterclockwise vortex is increasing in size and strength, the region of clockwise rotating fluid is decreasing. However, after the trailing-edge vortex is shed and convected downstream, the region of clockwise rotating fluid has enough space to extend in size until the next trailing-edge vortex is developing. In contrast to classical vortex shedding past bluff bodies showing well-established staggered arrangements of vortices of opposite sign and equal strength, for the airfoil at the present Re_c and α a highly asymmetric wake with vortices of unequal strength is observed. These observations are in close agreement with experimental findings for an inclined plate by Lam [34] and Perry & Steiner [35].

Additionally, Fig. 13 depicts the distribution of the total resolved Reynolds stresses ($\overline{u'u'}$, $\overline{v'v'}$, $\overline{u'v'}$) averaged in spanwise direction and time. All quantities include the periodic and the turbulent fluctuations. In order to separate both components, phase-averaging has to be carried out which is associated with several difficulties due to slightly varying shedding periods and is therefore omitted here. As expected, the largest values especially of $\overline{v'v'}$ are found in the vicinity of the trailing edge mainly caused by the quasi-periodic shedding motion of the trailing-edge vortex. In the entire low-pressure recirculation region the Reynolds stresses are very low

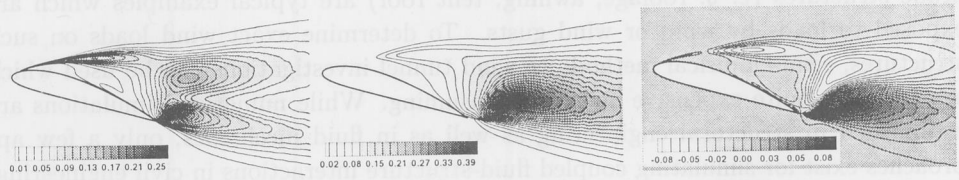

$\overline{u'u'}$ $\overline{v'v'}$ $\overline{u'v'}$

Figure 13. Distribution of resolved Reynolds stresses, $Re_c = 20{,}000$, $\alpha = 18^\circ$

with the exception of the shear layer region where the Kelvin-Helmholtz instability is observed. These plots strongly support the finding, that the asymmetric vortex structure past the inclined airfoil is dominated by the shedding mechanism at the trailing edge.

Simulations of the flow around an inclined flat plate at the same flow conditions (Breuer & Jovičić [18]) indicate very similar flow features as observed for the airfoil. Owing to the dominance of the trailing-edge vortex, this observation is not astonishing. In both cases the geometry of the trailing edge is only slightly different leading to comparable trailing-edge vortices and a similar shedding motion of these structures. This is also reflected by some integral parameters for both cases given in Table 1. Almost identical lift and drag coefficients ($\overline{C_l}$, $\overline{C_d}$) are found for the time-averaged flow. Concerning the fluctuations of the integral values given by standard deviations (σ_{C_l}, σ_{C_d}), slightly larger values are observed for the airfoil. The Strouhal number of the airfoil is only marginally smaller than for the flat plate ($\mathrm{St}' \approx 0.2$). This value is consistent with experimental findings for inclined thin plates which observed a nearly constant $\mathrm{St}' \approx 0.15$ for $20° \leq \alpha \leq 90°$ and a strong increase of $\mathrm{St}' \to 0.2$ for $\alpha \leq 20°$ (see, *e. g.*, Knisely [36] and the cited refs.).

Table 1. Comparison of important parameters for the airfoil and the flat plate

Configuration	$\overline{C_l}$	$\overline{C_d}$	σ_{C_l}	σ_{C_d}	St	St′
NACA-4415-Airfoil	1.118	0.391	$9.4 \cdot 10^{-2}$	$2.4 \cdot 10^{-2}$	0.636	0.197
Flat Plate	1.123	0.379	$6.9 \cdot 10^{-2}$	$2.2 \cdot 10^{-2}$	0.660	0.204

Fluid-structure interaction for a civil engineering application

The interaction of fluid and structure plays an important role in civil engineering. Besides bridges, towers or in general tall buildings also lightweight membrane structures (*e. g.* roofage, awning, tent roof) are typical examples which are exposed to loads by wind or wind gusts. To determine exact wind loads on such structures, semi-empirical methods or wind tunnel investigations can be used which are typically quite expensive and time-consuming. While numerical simulations are established in structural engineering as well as in fluid mechanics, only a few approaches exist for simulating coupled fluid-structure interactions in civil engineering. For that reason, a partitioned solution approach for the coupled problem is currently investigated [16] combining well-established and independently developed codes for **C**omputational **S**tructure **D**ynamics and CFD. The computation of the tensions and

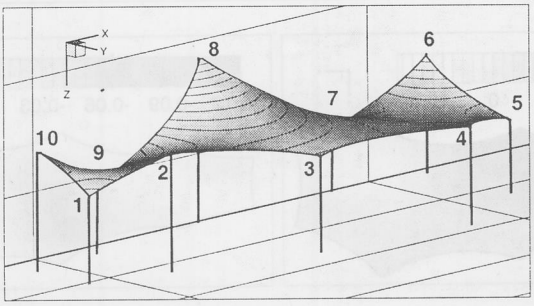

Figure 14. Tent structure in front of an office building

distortions in membrane structures such as textile roofs are based on an unstructured finite-element code ($\mathcal{ASE}$), where the simulation of the flow is based on the CFD code $\mathcal{FASTEST}$ explained above. The bilateral data exchange between both codes including the interpolation from the unstructured finite-element to the block-structured finite-volume grid and vice versa is managed by the MpCCI coupling interface [37] which internally utilizes the MPI library. Both codes run on their own node or number of nodes of the high-performance SMP cluster (Hitachi SR 8000-F1) after being spawned by a main process. The computational effort for the CFD part is generally much higher than for the CSD prediction. The pressure and the shear stress distribution on the tent structure obtained by the flow prediction are input data for the structure simulation, that provides the resulting displacement vector for the surface of the tent and the tensions inside the material. Based on the deformation of the structure, the CFD grid has to be adapted and in such a way a global iteration procedure is established typically leading to a globally converged deformation state within each time step after a few global iterations (*e. g.* 2–4).

Figure 14 shows an example for a textile canopy in front of an office building [16] recently constructed in Germany. The first test case was a RANS simulation of a *time-independent load* of the structure by wind blowing in positive x-direction with a strength of 11 on the Beaufort scale ten meters above the ground, which corresponds to a velocity of $u_\infty = 30$ m/s. An asymptotic behavior of the calculated wind load and displacement was found for this configuration during the global iterations leading to a steady deformation state, so that no time-dependent calculations were necessary. The final results for the pressure distribution on the upper side of the tent roof and the displacements in z-direction are also depicted in Fig. 15.

As a next example the superposition of a *constant basic wind flow* and a *time-dependent wind gust* was taken into consideration to realize an unsteady fluid-structure interaction [17]. The *basic flow* was assumed to be parallel to the ground in

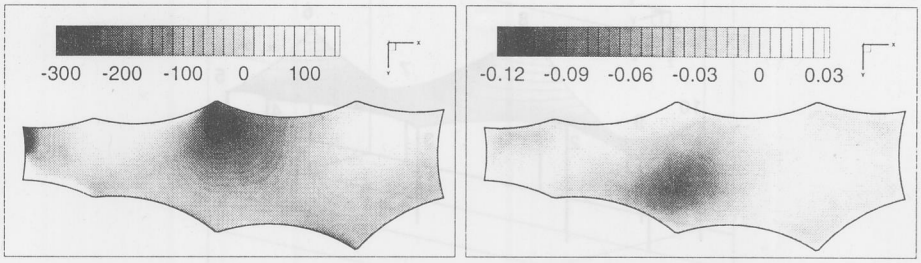

Figure 15. Computed pressure distribution on the upper side of the tent roof in Pa relative to atmospheric pressure (left), and computed displacements in z-direction in m (right) for a time-constant wind load

positive x-direction with $u_\infty = 10$ m/s in a height of 10 m above the ground. A *wind gust* was superimposed, which followed a Gaussian curve in time as well as in space:

$$W(x,t) = W_{\max}\, \mathrm{e}^{-0.5(t-t_\mathrm{m})^2}\, \mathrm{e}^{-0.005(x-x_\mathrm{m})^2}, \qquad (1)$$

with $x_\mathrm{m} = -12$ m and $t_\mathrm{m} = 3$ s. The vector of the inflow velocity is depicted in Fig. 16.

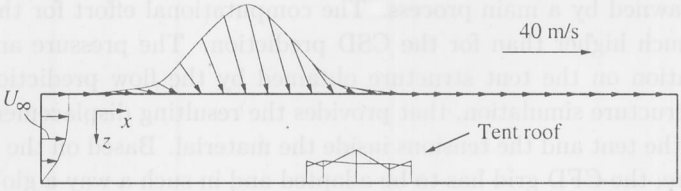

Figure 16. Illustration of the inflow velocity at time $t = t_m = 3$ s with velocity reference vector (to scale)

Figure 17 shows a sample of two states of the flow field as well as the structural deformations at two time instants. The grey scales on the walls represent the fluid velocity magnitude near the walls, while the shading of the membrane embodies its deformation. The largest deformation occured at the maximum of the wind gust at $t = 3$ s. A vertical displacement of $\Delta z_{\max} = 0.3$ m is observed approximately in the middle of the tent. Some of the surface points were moving upwards and others downwards during the impact of the gust. A few of them also showed a noticeable overshoot and subsequent small oscillations, before they reached the steady deformation state – which corresponds to the constant basic flow without superimposed wind gust – again.

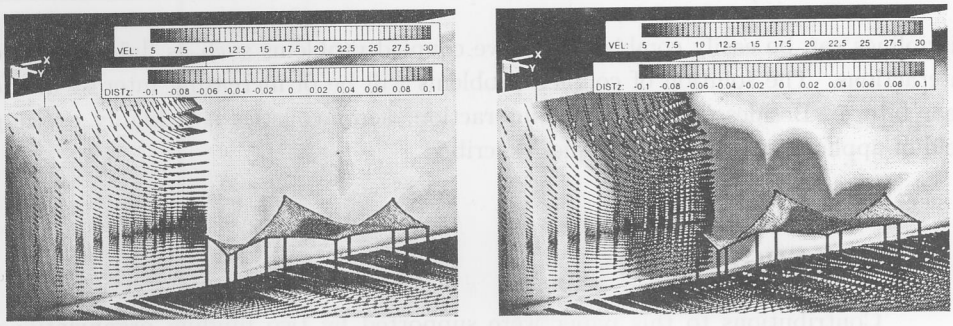

Figure 17. Velocity distributions displayed near the horizontal wall (ground) and the vertical wall (office building behind the membranous roof) and displacements displayed on the roof surface at two different time steps: $t_1 = 2.0$ s (left), $t_2 = 3.0$ s (right)

The mid-term objective of this investigation is to extend the flow prediction to *LES* and the structural simulation to *three-dimensional finite elements.*

CONCLUSIONS

Technological progress in one field typically has a strong impact on many other fields promoting developments which are otherwise not possible. This is especially true in the case of CFD and high-performance computers. Increased hardware performance combined with concurrent development of enhanced numerical methods triggered different fields of CFD, especially turbulence simulation. The present work has demonstrated that advanced techniques such as LES and DNS are suitable alternatives to the classical approach based on RANS with statistical models. Even for practically relevant complex turbulent flows, these approaches will at least partially replace RANS predictions in the near future. However, it should be clearly emphasized that these techniques should not be applied in zeal without knowledge to all kind of flow problems. However, if highly unsteady flows are dominated by complex flow phenomena such as separation, reattachment, transition or large-scale vortex motion, LES and DNS are often better suited than RANS. Despite the Reynolds number limitation of DNS, it is an extremely useful tool to study turbulent flows in detail. As shown in the present paper, these investigations are not restricted to simple geometries but can also be used in complex configurations. LES is in principle not limited in the Reynolds number range. Based on the circular cylinder and the airfoil flow, it was demonstrated that LES is able to predict complex turbulent flows at high Re with satisfactory accuracy. Finally, it was shown, how the development in different

disciplines can be easily combined to solve coupled problems such as fluid-structure interactions. The solution of coupled problems will be of increasing interest in the near future. Besides fluid-structure interaction, aero-acoustics is a highly exciting field of application for the techniques described.

ACKNOWLEDGEMENTS

Contributions to this paper were supported by two funding organizations, namely the *Deutsche Forschungsgemeinschaft* under contract number BR 1847/2 and the *Bayerische Forschungsstiftung* in the Bavarian Network of Competence for High-Performance Scientific Computing (KONWIHR) in the project *FLUSIB*. Additional financial support was also provided by NEC ESS (NEC Deutschland GmbH). The computations were carried out on a variety of high-performance computers. We have to mention the NEC SX-4 at the National Aerospace Laboratory (NLR), the NEC SX-4/5 of the High-Performance Computing Center Stuttgart, the Fujitsu VPP 700 of the Leibniz Computing Center, Munich, and last but not least the German Federal Top-Level Compute Server Hitachi SR 8000-F1 at HLRB, Munich. This support is also gratefully acknowledged.

REFERENCES

[1] Knight, K.E.: Changes in Computer Performance, Datamation, Sept. (1966), pp. 40

[2] Knight, K.E.: Evolving Computer Performance 1963–1967, Datamation, Jan. (1968), pp. 31

[3] Meuer, H.W., Strohmaier, E., Dongarra, J.J., Simon, H.D.: TOP500 Supercomputer Sites, 16th Edition, http://www.top500.org/, Nov. (2000)

[4] Breuer, M., Rodi, W.: Large-Eddy Simulation of Complex Turbulent Flows of Practical Interest, In: *Flow Simulation with High-Performance Computers II*, ed. E.H. Hirschel, *Notes on Numerical Fluid Mechanics*, vol. *52*, Vieweg, Braunschweig, (1996), pp. 258–274

[5] Breuer, M.: Large-Eddy Simulation of the Sub-Critical Flow Past a Circular Cylinder: Numerical and Modeling Aspects, *Int. J. Num. Methods Fluids*, vol. *28*, John Wiley & Sons Limited, Chichester, (1998), pp. 1281–1302

[6] Breuer, M.: Large-Eddy Simulation of High Reynolds Number Circular Cylinder Flow, Proc. of the Workshop on Indust. & Environ. Appl. of DNS and LES, Aug. 5–7, 1998, Boğaziçi Univ., Istanbul, Turkey, *Lecture Notes in Physics*, vol. *529*, Springer, (1999), pp. 176–189

[7] Breuer, M.: A Challenging Test Case for Large-Eddy Simulation: High Reynolds Number Circular Cylinder Flow, *Int. J. Heat Fluid Flow*, vol. *21*, no. 5, Elsevier Science B.V., Amsterdam, (2000), pp. 648–654

[8] Breuer, M., Bernsdorf, J., Zeiser, T., Durst, F.: Accurate Computations of the Laminar Flow Past a Square Cylinder Based on Two Different Methods: Lattice-Boltzmann and Finite-Volume, *Int. J. Heat Fluid Flow*, Elsevier Science B.V., Amsterdam, vol. *21*, no. 2, (2000), pp. 186–196

[9] Breuer, M.: Direct Numerical Simulation and Large-Eddy Simulation of Turbulent Flows with High-Performance Computers (in German), Habilitation Thesis, University of Erlangen-Nürnberg, Germany, (2001)

[10] Rodi, W., Ferziger, J.H., Breuer, M., Pourquié, M.: Status of Large-Eddy Simulation: Results of a Workshop, Workshop on LES of Flows Past Bluff Bodies, Rottach-Egern, Tegernsee, Germany, June 26–28, 1995, J. Fluids Engineering, vol. *119* (2), (1997), pp. 248–262

[11] Durst, F., Schäfer, M., Wechsler, K.: Efficient Simulation of Incompressible Viscous Flows on Parallel Computers, In: Flow Simulation with High-Performance Computers II, Notes on Numerical Fluid Mechanics, vol. *52*, Vieweg, Braunschweig, (1996), pp. 87–101

[12] Durst, F., Schäfer, M.: A Parallel Block-Structured Multigrid Method for the Prediction of Incompressible Flows, Int. J. Num. Methods Fluids, vol. *22*, (1996), pp. 549–565

[13] Wechsler, K., Breuer, M., Durst, F.: Steady and Unsteady Computations of Turbulent Flows Induced by a $4/45^o$ Pitched Blade Impeller, J. Fluids Engineering, vol. *121* (2), (1999), pp. 318–329

[14] Bartels, C., Breuer, M., Wechsler, K., Durst, F.: CFD-Applications on Parallel-Vector Computers: Computations of Stirred Vessel Flows, Int. J. Computers and Fluids, vol. *31*, no. 1, Elsevier Science Ltd, Oxford, (2001), pp. 69–97

[15] Bartels, C., Breuer, M., Durst, F.: Comparison between Direct Numerical Simulation and k-ε Model Prediction of the Flow in a Vessel Stirred by a Rushton Turbine, *10th European Conference on Mixing*, Delft University of Technology, The Netherlands, July 2–5, (2000)

[16] Glück, M., Breuer, M., Durst, F., Halfmann, A., Rank, E.: Computation of Fluid-Structure Interaction on Lightweight Structures, Int. J. of Wind Engineering and Industrial Aerodynamics, vol. *89*, no. 14–15, (2001), pp. 1351–1368

[17] Glück, M., Breuer, M., Durst, F., Halfmann, A. & Rank, E.: Computation of Wind-Induced Vibrations of Flexible Shells and Membranous Structures, subm. to J. of Fluids and Structures, (2001)

[18] Breuer, M., Jovičić, N.: Separated Flow Around a Flat Plate at High Incidence: An LES Investigation, Second Int. Symposium on Turbulence and Shear Flow Phenomena, Stockholm, Sweden, June 27–29, 2001, vol. *III*, pp. 393–398, J. of Turbulence, vol. **2**, pp. 1–15, (2001)

[19] Breuer, M., Jovičić, N.: An LES Investigation of the Separated Flow Past An Airfoil at High Angle of Attack, Proc. of the 4th Workshop on Direct and Large-Eddy Simulation, Enschede, The Netherlands, July 18–20, 2001, ERCOFTAC Series, vol. **8**, pp. 165–172, Direct and Large-Eddy Simulation IV, eds. B.J. Geurts, R. Friedrich, O. Métais, Kluwer Academic Publishers, Dordrecht, (2001)

[20] Rhie, C., Chow, W.: Numerical Study of the Turbulent Flow Past an Airfoil with Trailing Edge Separation, AIAA J., vol. *21*, (1983), pp. 1525–1532

[21] Smagorinsky, J.: General Circulation Experiments with the Primitive Equations, I, The Basic Experiment, Mon. Weather Rev., vol. *91*, (1963), pp. 99–165

[22] Germano, M., Piomelli, U., Moin, P., Cabot, W.H.: A Dynamic Subgrid Scale Eddy Viscosity Model, *Phys. Fluids A*, vol. *3* (7), (1991), pp. 1760–1765

[23] Lilly, D.K.: A Proposed Modification of the Germano Subgrid-Scale Closure Method, *Phys. Fluids A*, vol. *4* (3), (1992), pp. 633–635

[24] Harvey, A.D., Lee, C.K., Rogers, S.E.: Steady-State Modeling and Experimental Measurement of a Baffled Impeller Stirred Tank, *AIChE J.*, vol. *41*, (1995), pp. 2177–2186

[25] Brehm, M., Bader, R., Ebner, R.: High-Performance Computers in Bavaria (HLRB): The Hitachi SR 8000-F1 (in German), `http://www.lrz-muenchen.de/services/compute/hlrb/`, (2001)

[26] Leister, H.J., Perić, M.: Vectorized Strongly Implicit Solving Procedure for a Seven-Diagonal Coefficient Matrix, *Int. J. Heat Fluid Flow*, vol. *4*, (1993), pp. 159–172

[27] Schäfer, M., Höfken, M., Durst, F.: Detailed LDV Measurements for Visualization of the Flow Field within a Stirred-Tank Reactor Equipped with a Rushton Turbine, *Trans. IChemE*, vol. *75*(A), (1997), pp. 729–736

[28] Rushton, J.H., Costich, E.W., Everett, J.J.: Power Characteristics of Mixing Impellers – Part II, *Chem. Eng. Progress*, vol. *46* (9), (1950), pp. 467–476

[29] Rutherford, K., Mahmoudi, S.M.S., Lee, K.C., Yianneskis, M.: The Influence of Rushton Impeller Blade and Disk Thickness on the Mixing Characteristics of Stirred Vessels, *Trans. IChemE*, vol. *74* (A), (1996), pp. 369–378

[30] Schäfer, M., Wechsler, K., Durst, F.: Advanced Methods for Investigation of Single-Phase Stirred Vessel Flows. Part I: Experimental Methods. *Proc. of AIChE Annual Meeting*, Miami Beach, FL, USA, Nov. 1997, American Institute of Chemical Engineers, (1998)

[31] Cardell, G.S.: Flow Past a Circular Cylinder with a Permeable Splitter Plate, Ph.D. Thesis, Graduate Aeronautical Lab., California Inst. of Technology, (1993)

[32] Cantwell, B., Coles, D.: An Experimental Study on Entrainment and Transport in the Turbulent Near Wake of a Circular Cylinder, *J. Fluid Mechanics*, vol. *136*, (1983), pp. 321–374

[33] Lerche, Th., Dallmann, U. Ch.: The Basic Experiment COSTWING I: Documentation of the Set-Up Phase (in German), Inst. f. Strömungsmechanik, DLR Göttingen, Germany, IB 223–99 A04, (1999)

[34] Lam, K.M.: Phase-Locked Eduction of Vortex Shedding in Flow Past an Inclined Flat Plate, *Phys. of Fluids*, vol. *8* (5), (1996), pp. 1159–1168

[35] Perry A.E., Steiner, T.R.: Large-Scale Vortex Structures in Turbulent Wakes Behind Bluff Bodies, Part 1: Vortex Formation Process, *J. of Fluid Mechanics*, vol. *174*, (1987), pp. 233–270

[36] Knisely, C.W.: Strouhal Numbers of Rectangular Cylinders at Incidence: A Review and New Data, *J. of Fluids and Structures*, vol. *4*, (1990), pp. 371–393

[37] Ahrem, R., Hackenberg, M.G., Post, P., Redler, R. & Roggenbuck, J.: MpCCI – Mesh Based Parallel Code Coupling Interface, Institute for Algorithms and Scientific Computing (SCAI), GMD, `http://www.mpcci.org/`, (2000)

Authors address:

M. Breuer, M. Glück, N. Jovičić, C. Bartels
Institute of Fluid Mechanics
University of Erlangen-Nürnberg
Cauerstr. 4, D-91058 Erlangen
Germany

Paper submitted: November 30, 2001
Paper revised: February 26, 2002
Paper accepted: March 18, 2002